# An Eight-Element Reconfigurable Diversity Dipole System

Youssef Tawk, Joseph Costantine, and Christos G. Christodoulou, *Fellow, IEEE*

***Abstract*— In this paper, an antenna system that is composed of eight radiating elements is presented. The eight elements consist of a set of four curved dipoles and another set of four straight dipoles, providing two diversity antenna structures. Each curved and straight dipole is designed to produce a focused gain pattern toward one dedicated quadrant. A parasitic printed reflector is introduced into the center section of the top layer of the proposed antenna to enhance the matching and the gain pattern redirection capabilities of each radiating element. In addition, the printed reflector further enhances the isolation between the various elements. The assessment of the proposed diversity antenna system is performed in a rich multipath environment for various propagation scenarios. A diversity gain between 16.5 and 19.1 dB is attained for a 1% probability level and by assuming a Rayleigh fading channel for both structures. The control of the feeding of the various elements for both diversity structures is achieved through the design and incorporation of four reconfigurable feeding networks within the antenna system. Fabrication and testing of various prototypes display very good agreement between the simulation and measured results, which validate the presented designs.**

***Index Terms*— Antenna diversity, dipole antenna, frequency reconfigurability, MIMO system, pattern diversity, polarization orthogonality, reconfigurable antenna.**

## I. Introduction

DIVERSITY antenna structures are required for next generation wireless systems to provide high data rates and increased channel capacity. Several antenna concepts have been presented in the literature with diversity behavior [1]–[12]. A four ports wideband antenna that is able to radiate two broadside patterns and two omnidirectional patterns is presented in [1]. Another antenna structure that features two orthogonal and one diagonal linear polarization is discussed in [3]. The proposed structure can also achieve beam switching for the three different polarization states by electrically reconfiguring specific parasitic elements.

The improvement in the gain characteristics of printed antenna structures is an added feature for diversity systems [12]–[18]. One possible implementation is the loading of shorting pins to disrupt the field distributions beneath the radiating patch [13]. Another possible implementation is to incorporate a set of parasitic elements that serve as director cells. For example, in [15], parasitic elements are added to the shorter end of a printed log-periodic dipole array in order to achieve gain enhancement.

The performance of a diversity antenna structure is highly dependent on the isolation between the various radiating elements. An extensive work can be found in the literature that proposes different techniques to improve the isolation levels between the different radiating elements [19]–[26]. A coupled resonator decoupling network is presented in [20] to reduce the mutual coupling between two dual-band antennas operating at 2.4 and 5.2 GHz. Zhai *et al.* [21] propose the integration of a wall with a double metamaterial mushroom like structure between the four antenna elements. Each element is probe fed and is composed of a substrate-integrated cavity backed slot. An enhanced interelement isolation of 16 dB is achieved between the parallel-directed antenna element pairs.

The addition of frequency reconfigurability to a diversity antenna structure is instrumental in a dynamic environment such as cognitive radio [27]. In such environment, the users' activity is constantly monitored through a sensing antenna and the communicating antenna is reconfigured accordingly. One possible implementation is to design a reconfigurable feeding network that changes the operating frequency of the various elements on demand [28]–[31]. For example, in [29], a reconfigurable feeding network using p-i-n diodes is proposed. The network is able to provide four different transmission modes and is composed of coupled line sections in order to miniaturize the size as well as enhance the coupling between the ports. It is essential to note that the reconfiguration can also be obtained by relying on various electrical switches other than p-i-n diodes [32].

In this paper, the design of a radiating system that is composed of two diversity antenna structures is presented [33], [34]. Each diversity antenna structure is composed of four elements that operate over a different span of frequencies with a directive gain pattern. Two elements are aligned along the $x$-axis while the others two are placed along the $y$-axis to provide orthogonal polarization between the various radiating elements. A set of four curved dipoles constitute the first diversity structure while the second diversity structure is composed of four straight dipoles.

The novelty of the presented paper is based on the compact integration of the two antenna structures. Each structure is appropriately designed to actively shape the gain pattern of the other structure while at the same time enhance the

Manuscript received January 8, 2017; revised September 6, 2017; accepted November 17, 2017. Date of publication December 7, 2017; date of current version February 1, 2018. *(Corresponding author: Youssef Tawk.)*

Y. Tawk is with the Electrical and Computer Engineering Department, Notre Dame University, Louaize, 72 Zouk Mikael, Lebanon (e-mail: yatawk@ieee.org).

J. Costantine is with the Electrical and Computer Engineering Department, American University of Beirut, Beirut 1107 2020, Lebanon (e-mail: jcostantine@ieee.org).

C. G. Christodoulou is with the Electrical and Computer Engineering Department, University of New Mexico, Albuquerque, NM 87131 USA (e-mail: christos@unm.edu).

Color versions of one or more of the figures in this paper are available online at http://ieeexplore.ieee.org.

Digital Object Identifier 10.1109/TAP.2017.2780894

isolation levels. The novelty of this paper is also focused on the simple feeding of the different dipoles through the integration of a multilayer surface mount chip balun in addition to the incorporation of a printed parasitic reflective surface in the empty space between the dipoles. Such integration contributes to the compactness of the design and enhances the isolation as well as the directive characteristics of the whole antenna system. The novelty of this paper can also be assessed by the selective activation of each diversity antenna structure. Four reconfigurable feeding networks are placed underneath the antenna's bottom layer and orthogonally to the printed curved reflector. Such selectivity enables the entire antenna diversity system to reconfigure its operating frequency. The proposed antenna system in this paper can be adopted in a cognitive radio environment. Radiation diversity along with frequency reconfiguration is needed features in a cognitive radio system. The two diversity structures can be activated based on the users' activity in the channel while applying a cognition ability to the system. Such performance enhances the spectrum usage efficiency and guarantees a high tolerance of multipath effects due to the diversity performance of the proposed antenna system.

Section II discusses the design of a dual antenna system that is composed of one curved and one straight dipole. The implementation of the whole antenna system is detailed in Section III. The addition of the printed parasitic reflector is presented in Section IV. The assessment of the fabricated prototype is highlighted in Section V. The analysis of the antenna system in a multipath environment is investigated in Section VI. The control of the elements' radiation characteristics through the integration of a reconfigurable feeding network is discussed in Section VII. Concluding remarks are drawn in Section VIII.

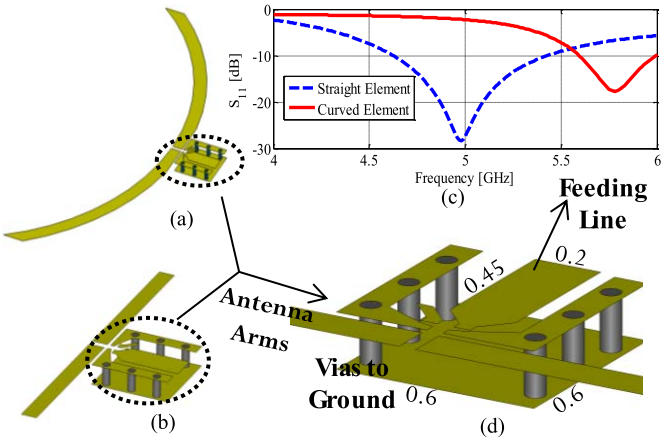


Fig. 1. (a) Curved dipole structure. (b) Straight dipole. (c) Reflection coefficient for both structures. (d) Balun circuitry.

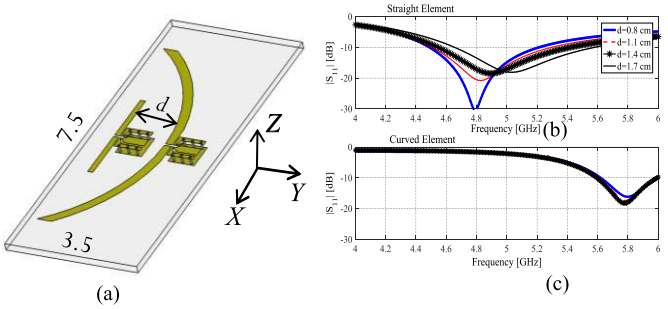


Fig. 2. (a) Integration of both radiating elements. Reflection coefficients for the (b) straight dipole and (c) curved dipole.

## II. Dual Antenna Element Integration

The design process of the complete antenna system is initiated by integrating two antenna elements in close proximity to each other. The two antennas are composed of a straight and curved dipoles. The purpose of such integration is to investigate the ability of one antenna structure, when inactive, to act as a parasitic reflector to the other active antenna. Fig. 1(a) shows the structure of the curved dipole printed on top of Rogers 5880 substrate with a dielectric constant of 2.2 and a thickness of 1.6 mm. The length of the dipole (65.4 mm) corresponds to almost $3\lambda_g/2$ at $f = 5.8$ GHz. $\lambda_g$ is the guide wavelength that takes into account the fringing effect inside the dielectric substrate. The width of each dipole arm is designed to be 3.279 mm for a differential input impedance of 50 Ω. The structure of the straight dipole is shown in Fig. 1(b). This structure has a length of 23.325 mm and a width of 1.2 mm in order to operate at 5 GHz with also a differential input impedance of 50 Ω. The straight dipole resonates at almost $\lambda_g/2$. The reflection coefficients for both radiating structures are summarized in Fig. 1(c) displaying the antennas' respective frequencies of operation. The excitation mechanism of both elements is highlighted in Fig. 1(d). A six-pin surface mount multilayer chip balun is used to feed the two arms of each dipole [35]. The balun provides the appropriate transition from the dipole's balanced structure to the unbalanced antenna feeding point by providing a phase difference of 180° between the two arms of each dipole. It also allows the appropriate transformation from an input impedance of 50 Ω to a differential impedance of 50 Ω between the dipole arms. Two pins of the integrated balun are connected to the two arms of the dipoles. Two other pins are connected to the balun's ground through six vias. The ground has a dimension of 0.6 cm × 0.6 cm. One pin is connected to the antenna's SMA connector through the feeding line that has a length of 0.45 cm and a width of 0.2 cm.

The two dipole structures are then integrated together, as shown in Fig. 2(a), on the same antenna substrate with a total dimension of 7.5 cm × 3.5 cm. The distance of separation $d$ between the two radiating elements is optimized for a minimum effect on their matching and gain charactertistics. The presence of the curved dipole has an inductive effect on the input impedance of the straight dipole. Without the presence of the curved dipole, the reactive component of the input impedance of the straight dipole is $-j0.37$ Ω at 5 GHz. However, after the integration ($d = 0.8$ cm), the reactive part changes to $+j21.725$ Ω at 5 GHz. This change forces the straight dipole to shift its resonant frequency to 4.8 GHz while maintaining the same physical length. The reflection coefficient of the straight dipole is shown in Fig. 2(b) for different values of $d$. The best matching is obtained when $d = 0.8$ cm with an operation that shifts from 5 to 4.8 GHz.

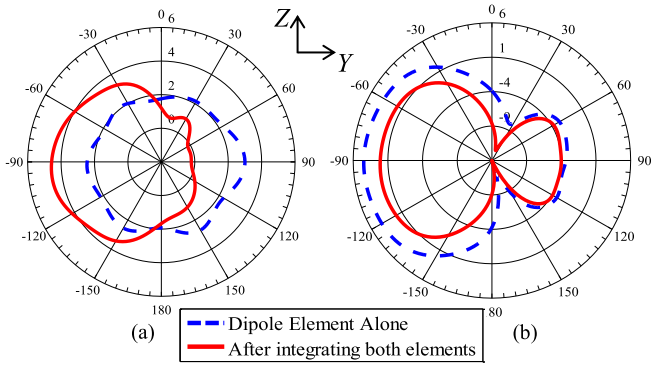


Fig. 3. Change in the total gain pattern for the (a) straight dipole (dashed line: 5 GHz/solid line: 4.8 GHz) and (b) curved dipole (dashed and solid lines: 5.8 GHz).

The effect of the straight dipole on the reflection coefficient of the curved element is negligible, as shown in Fig. 2(c), for different values of $d$. It is clear that the curved dipole preserves almost the same reflection coeffecient. This is related to the fact that the straight dipole is shorter in length and its parasitic effect is not noticeable on the curved dipole's input impedance. For the remainder of this paper, the distance $d = 0.8$ cm is kept between the two dipoles.

The change in the total gain pattern of the straight dipole antenna in the $yz$ plane is highlighted in Fig. 3(a). The pattern changes from omnidirectional to a directive one. The curved dipole element forces the radiated fields by the straight dipole to be directed toward one direction ($-y$-direction) and blocks the radiation from the opposite direction ($+y$-direction). The maximum total gain increases from 2.9 dBi at $f = 5$ GHz (standalone) to 4.5 dBi at $f = 4.8$ GHz (dual). As for the back lobe gain (at $\theta = 90°$), its value drops from 2.9 to $-0.2$ dBi.

The curved dipole by itself produces a directional pattern with a maximum realized gain of 4.45 dBi and a front to back gain ratio of 8.18 dB. The parasitic effect of the straight dipole on the total gain pattern of the curved element is shown in Fig. 3(b). Such effect is noticed by a drop of almost 2 dB in the maximum realized gain as well as in the front to back gain ratio. Such drop is obtained since the close proximity to the straight dipole affects the curved element radiation efficiency and thus adds destructively to the total realized gain pattern. This can be solved by changing the distance of separation $d$ between the two elements. However, this will disturb the performance of the straight dipole. Another solution will be discussed in Section IV to restore the curved dipole's gain witout impacting the straight dipole's impedance matching and gain levels.

## III. Eight-Element Antenna Structure

In this section, the dual antenna integration is extended into an eight-element antenna system with dual frequency of operation, directive gain pattern as well as dual polarization. The eight elements are placed along the four edges of the antenna substrate, as shown in Fig. 4. The antenna susbtrate is placed along the $xy$ plane (horizontal plane). For each structure, two elements are oriented along the $x$-axis while the other two are placed along the $y$-axis. Such placement

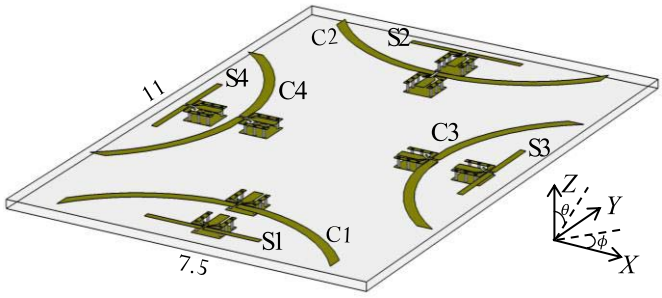


Fig. 4. Diversity antenna structure composed of eight radiating elements.

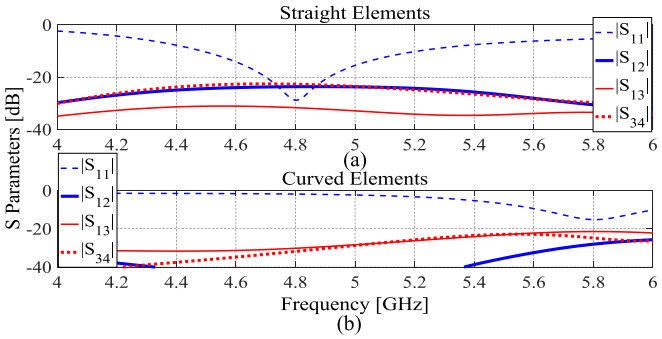


Fig. 5. Simulated S-parameters between the various (a) straight dipoles and (b) curved dipoles.

enables the antenna to feature an orthogonal polarization behavior by receiving both linearly polarized waves along the $x$- and $y$-directions. The dimension of the antenna's Rogers 5880 substrate is 11 cm × 7.5 cm. The two straight dipoles Element 1: S1 and Element 2: S2 are separated by a distance of 8.3 cm while Element 3: S3 and Element 4: S4 are separated by a distance of 5.1 cm. As for the second structure, the two curved dipoles (C1 and C2) are separated by a distance of 5.9 cm while C3 and C4 are separated by a distance of 2.7 cm. The various distances are greater than the corresponding quarter wavelength at the dipole's resonant frequency [36].

The reflection coefficient of any straight dipole in addition to the isolation between S1 and S2, S1 and S3 as well as S3 and S4 are included in Fig. 5(a). The straight dipole preserves its operation at 4.8 GHz. A good level of isolation is obtained between the various elements due to two factors. First, the distance of separation between the different dipoles is greater than quarter wavelength and second each straight dipole produces a directional pattern due to the presence of the corresponding curved dipole. The best isolation ($-32$ dB) is obtained between S1 and S3 since one element is placed along the $x$-direction while the other is along the $y$-direction.

The corresponding S-parameters results for the curved dipoles are shown in Fig. 5(b). Each curved element resonates at 5.8 GHz. An isolation below $-20$ dB is obtained between the various elements due to the directional pattern of each curved dipole as well as the corresponding distance of separation. The lowest isolation is obtained between C1 and C3 despite their orthogonal polarization. This behavior is related to the close proximity between these two elements. It is important to note that for either the curved or

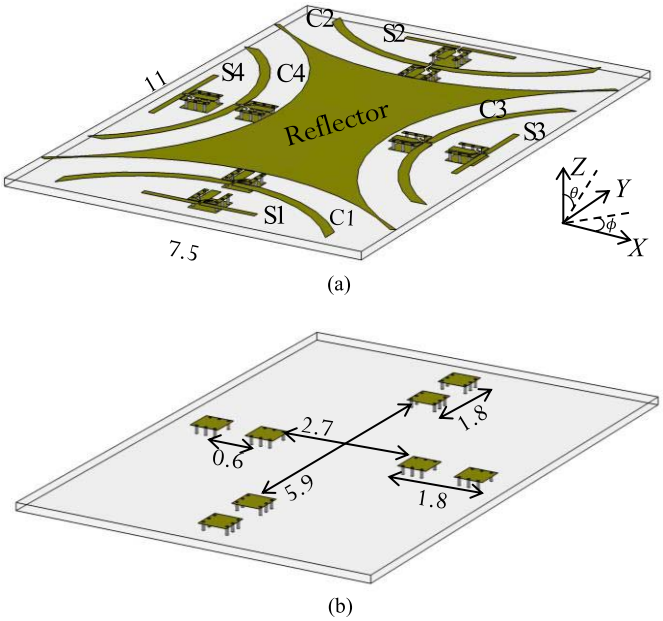


Fig. 6. Final antenna structure after the integration of the printed parasitic element. (a) Top view. (b) Bottom view.

straight dipoles, the isolation levels between elements 1 and 3, elements 3 and 2, or elements 2 and 4 are identical. In terms of the total gain pattern, each dipole element preserves almost the same characteristics as the dual antenna system. A directive gain pattern toward one of the four quadrants is now achieved. These four quadrants are divided as follows between the various dipole elements for $-180° < \theta < 180°$.

*Quadrant 1* ($0° < \phi < 45°$ and $315° < \phi < 360°$) is dedicated for C3 and S3.
*Quadrant 2* ($45° < \phi < 135°$) is dedicated for C2 and S2.
*Quadrant 3* ($135° < \phi < 225°$) is dedicated for C4 and S4.
*Quadrant 4* ($225° < \phi < 315°$) is dedicated for C1 and S1.

## IV. Integration of a Printed Parasitic Reflector

The performance of the antenna system discussed in Section III is further enhanced through the integration of a parasitic printed reflector in the center of the top layer, as shown in Fig. 6. The four edges of the parasitic element have the same curvature and almost the same length as the curved dipoles. Such addition forces each antenna element in the two diversity structures to produce a more directive gain pattern. It also compensates for the drop in the gain levels of the curved dipoles. It is important to note that the addition of this parasitic element does not increase the total dimensions of the antenna system since it is placed in the empty space between the four curved elements.

### *A. Effect on the Input Reflection Coefficient of any Curved and Straight Dipole*

The effect of the printed reflector on the reflection coefficient of any straight and curved dipole is shown in Fig. 7(a). The resonant frequency of the curved dipole is shifted from 5.8 to 5.6 GHz. This is due to the inductive effect of the printed parasitic element on the impedance of any curved dipole.

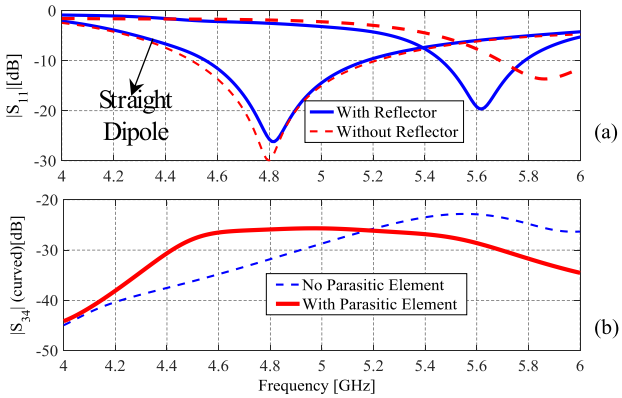


Fig. 7. (a) Effect of the printed parasitic reflector on the reflection coefficient of both radiating structures. (b) Change in the isolation between C3 and C4.

The impedance match of the curved dipole is also improved where the reflection coefficient drops from −15 dB at 5.8 GHz to −20 dB at 5.6 GHz. The reflection coefficient of any straight dipole is also included in Fig. 7(a). The straight dipole preserves its resonant frequency at 4.8 GHz. This is obtained since the existence of the curved dipole minimizes the effect of the parasitic element on the impedance of the straight dipole.

### *B. Effect on the Isolation Between the Curved Dipoles*

The improvement in the isolation between the curved dipoles C3 and C4 can be inspected in Fig. 7(b). The isolation level at $f = 5.6$ GHz is almost −30 dB after adding the curved parasitic element. On the other hand, the isolation between the curved dipole C1 and C3 remains almost the same. The same behavior applies to the other combination of the curved dipole elements.

### *C. Effect on the Gain Pattern of the Curved/Straight Dipoles*

The realized total gain pattern for the two curved dipole elements C3 and C4 after the integration of the printed reflector is plotted in Fig. 8(a) along the $xz$ plane at $f = 5.6$ GHz. The gain pattern becomes more directive with a maximum realized gain of 6.7 dBi and a minimal back lobe. The front to back gain ratio has improved from 5.98 dB without the printed parasitic element to almost 12 dB. The total gain pattern at $f = 4.8$ GHz for S3 and S4 is summarized in Fig. 8(b) along the $xz$ plane. The back lobe gain pattern is reduced from −0.2 dBi (without the parasitic reflector) to almost −8 dBi. As for the peak gain, it retains its maximum value of 4.7 dBi. Fig. 8(c) shows the 3-D total gain pattern when C3/C4 is activated, while Fig. 8(d) presents the same data when S1/S2 is fed. These two plots highlight the directive behavior of the total gain pattern after the integration of the printed parasitic reflector. Each dipole is dedicated to cover a specific quadrant.

### *D. Effect on the Polarization of the Curved/Straight Dipoles*

Fig. 9 shows the cross-polarized gain component for S1/C1 and the co-polarized gain component for S4/C4 in

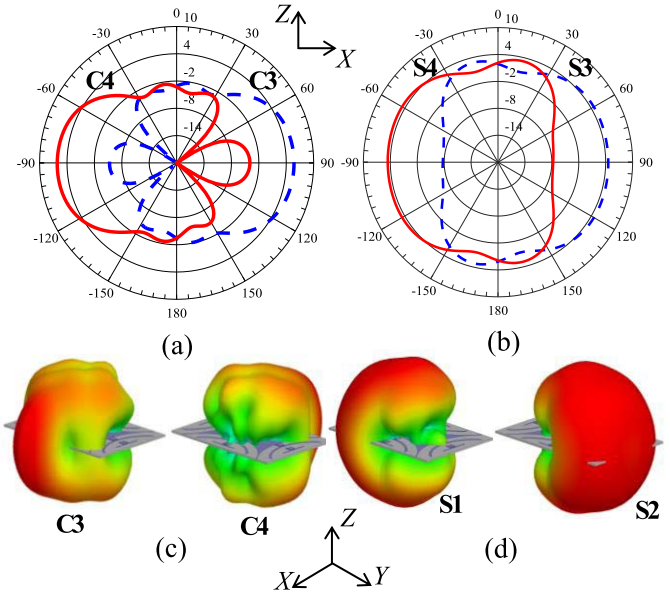


Fig. 8. Total gain pattern after the addition of the printed parasitic element for (a) C3 and C4 ($f = 5.6$ GHz) and (b) S3 and S4 ($f = 4.8$ GHz). (c) 3-D gain pattern when C3 or C4 is activated ($f = 5.6$ GHz) and (d) S1 or S2 is activated ($f = 4.8$ GHz).

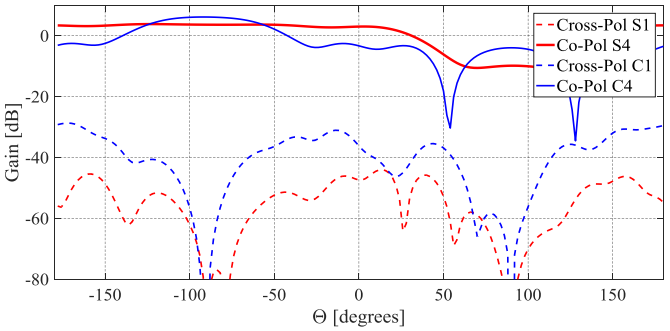


Fig. 9. Gain difference between the cross-polarized component of S1/C1 and the co-polarized component of S4/C4.

the $xy$ plane. Even though the four polarizations components shown in Fig. 9 possess the same sense ($y$-polarized), a noticeable gain difference is obtained between the two straight as well as the two curved elements. Similar results can be obtained between the remaining dipoles. These results confirm that the polarization orthogonality feature is maintained for both structures. Such behavior is mainly related to the placement of the various elements along the four edges of the substrate.

## V. Assessment of the Fabricated Prototype

The proposed antenna system is fabricated to test its performance, as shown in Fig. 10. Every integrated balun has a ground plane that is optimized to be of the same size as the connector. A hole is drilled throughout the substrate to connect the feeding point to the input lead of the balun. The comparison between the simulated and measured antenna's reflection coefficients when one curved dipole is fed while all the other elements are loaded by 50 Ω terminations is shown in Fig. 11. Any curved dipole element covers a measured band in the 5.3–5.85 GHz range. The same mechanism is

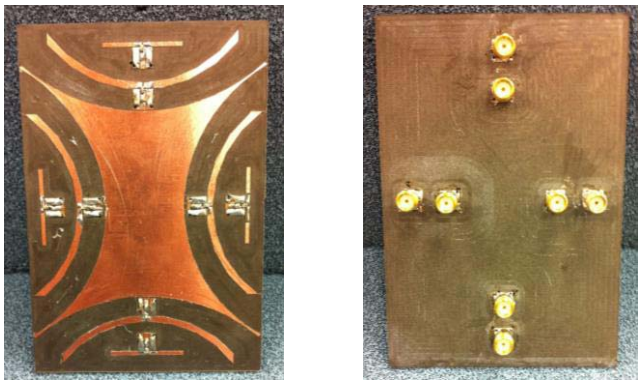

Fig. 10. Top and bottom layers of the fabricated prototype.

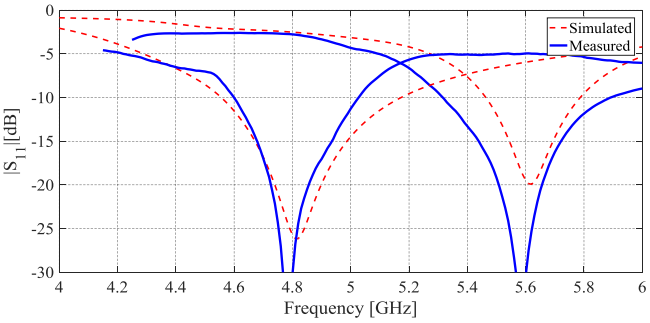


Fig. 11. Reflection coefficient of any curved dipole and straight dipole.

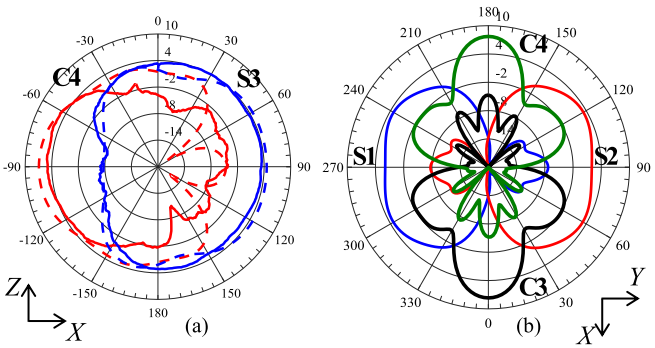


Fig. 12. (a) Simulated (dashed line) and measured (solid line) total gain pattern in the $xz$ plane for S3 at $f = 4.8$ GHz and C4 at $f = 5.6$ GHz. (b) Measured gain for S1, S2, C3, and C4 in the $xy$ plane.

repeated by feeding only one straight dipole and terminating the remaining seven elements by 50 Ω. Any straight dipole element covers the band of frequency from 4.6 to 5 GHz as also presented in Fig. 11. For both measurements, a good agreement is noticed with the computed data.

The simulated and measured total gain pattern in the $xz$ plane are plotted in Fig. 12(a) for the case when S3 ($f = 4.8$ GHz) or C4 ($f = 5.6$ GHz) is fed. The patterns for the other straight or curved dipoles are similar but with the main beam directed in other directions according to their respective positions on the antenna system. A measured maximum total gain of 4.5 dBi (S3) and 5.6 dBi (C4) is achieved accordingly. To further investigate the directive behavior of the proposed antenna system, the total measured gain pattern in the $xy$ plane is summarized in Fig. 12(b) for the two straight dipoles (S1 and S2) as well as for the two curved

TABLE I

MEASURED ISOLATION $|S_{ij}|$ BETWEEN THE VARIOUS ELEMENTS IN THE TWO RADIATING STRUCTURES

| Straight Dipoles ($f$=4.8 GHz) | Curved Dipoles ($f$=5.6 GHz) |
|---|---|
| $\|S_{12}\|_{dB}$=-41 | $\|S_{12}\|_{dB}$ =-31 |
| $\|S_{13}\|_{dB}$ =-30 | $\|S_{13}\|_{dB}$ =-28 |
| $\|S_{34}\|_{dB}$ =-28 | $\|S_{34}\|_{dB}$ =-28 |

TABLE II

DIVERSITY GAIN FOR BOTH RANDOM-LOS AND RIMP SCENARIOS BETWEEN VARIOUS TWO-DIPOLE ELEMENTS

| Radiating Elements | Random-LOS | RIMP |
|---|---|---|
| C1-C2/**S1-S2** | 10.2/**7.2** | 11.5/**11.7** |
| C3-C4/**S3-S4** | 7.6/**10.6** | 11.8/**11.7** |
| C2-C3/**S2-S3** | 8.9/**7.4** | 11.7/**11.6** |

dipoles (C3 and C4). Such plot proves that each straight/curved dipole element covers a specific quadrant with a minimal back lobe radiation. The measured isolation between the various straight as well as curved dipoles are summarized in Table I. The fabricated antenna structure is able to maintain low isolation levels between the different elements. These values agree well with the simulated data presented in Section IV.

## VI. DIVERSITY SYSTEM ANALYSIS

The proposed antenna system can be deployed in a multiple-input-multiple output (MIMO) environment with dual operating frequency, directive radiation patterns and dual polarization. The antenna system can be considered as a two four-element MIMO structure. The first structure is composed of the straight elements while the second one consists of the curved elements. It is important to note that the whole antenna system is placed along the *xy* plane (horizontal plane), as detailed in Fig. 6. For both diversity structures, there are four branches where each branch corresponds to one of the radiating elements.

The diversity gain of the proposed structure is first assessed in a random-line of sight (LOS) as well as rich isotropic multipath (RIMP) propagation environments [38]–[40]. These two scenarios are studied since real-life environments are somewhere in between a random-LOS and an RIMP. Thus, if an antenna structure exhibits good performance in these two environments, it will also perform well under real-life conditions [41]. The diversity gain between two various dipole elements for both scenarios is summarized in Table II. It is found that the gain varies between 7.2 and 11.7 dB. This gain level increases when considering the four curved/straight dipole elements. Fig. 13(a) shows the diversity gain between the four curved dipoles in a random-LOS environment while Fig. 13(b) presents the case for the four straight dipoles for the RIMP scenario. A diversity gain of almost 16.5/18.9 dB is achieved for the four curved dipoles (random-LOS/RIMP) while the four straight dipoles feature a diversity gain of 16.7/19.1 dB (random-LOS/RIMP). The diversity gain is calculated for a 1% probability level and by assuming a Rayleigh fading channel with the average noise being equal and uncorrelated between the antenna branches. Such level of diversity gain is obtained due to the high isolation between the dipole elements as

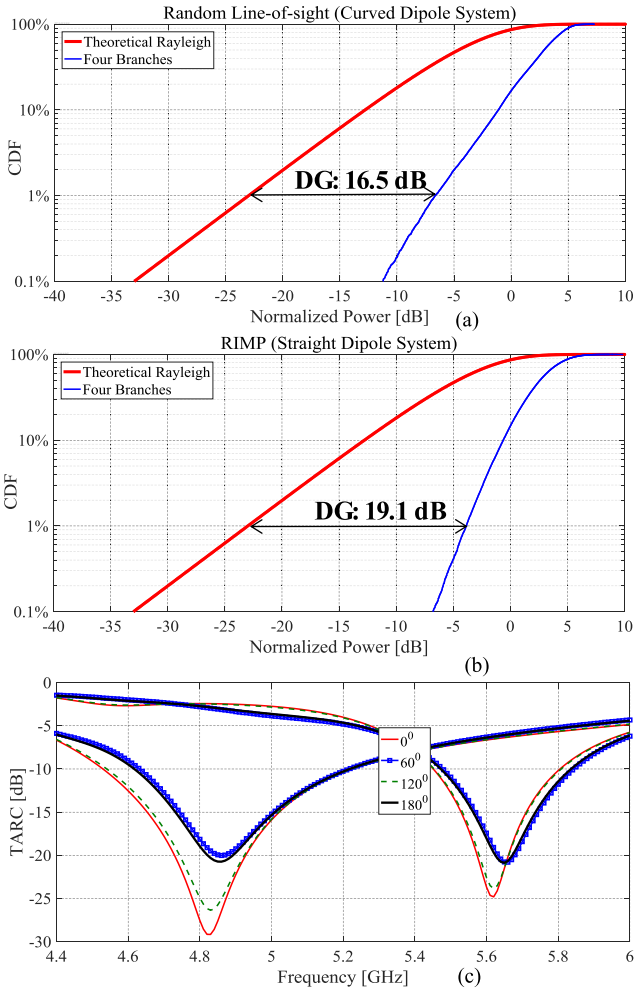


Fig. 13. Cumulative distribution function for the (a) four curved dipoles (random-LOS) and (b) four straight dipoles (RIMP). (c) TARC between S1 and S2 as well as C1 and C2 for various phase differences.

well as the directive gain pattern of the curved and straight dipoles. These results prove the validity of the proposed antenna structure as a diversity structure in a high multipath environment.

The envelope correlation coefficient, mean effective gain (MEG) of each branch, and the MEG ratio between the diversity branches for both dipole structures verify the required limits for a suitable MIMO behavior. Such MIMO behavior is evaluated in various statistical distribution of the incoming signals (Gaussian, Laplacian, and elliptical) [42]–[44]. The analysis performed proves that for the three different channel models in both indoor and outdoor environments, the two structures are able to exhibit an independence between the different incoming fading signals in a multipath environment and thus satisfy all the required MIMO constraints.

Another parameter to take into consideration in such analysis is the total active reflection coeffection (TARC). The objective of such study is to ensure that the power delivered to each dipole element is radiated. The TARC determines the resonant frequency and the impedance bandwidth of the MIMO structure as a function of the phase excitation between the various dipole elements. The TARC (dB) between S1 and S2 as well as between C1 and C2 are shown in Fig. 13(c) for four different

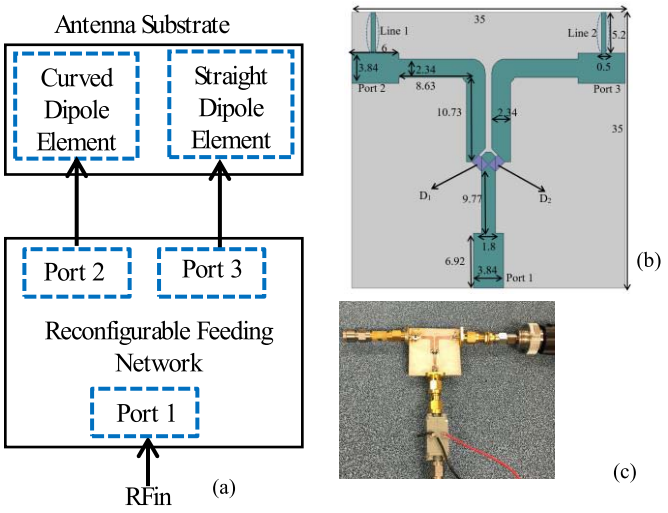


Fig. 14. (a) Control of two different radiating elements via a reconfigurable feeding network. (b) Physical dimensions of the proposed reconfigurable feeding network. (c) Fabricated prototype.

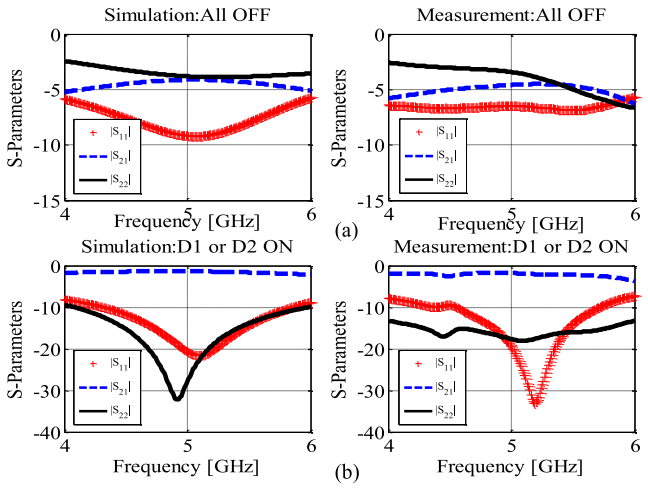


Fig. 15. Comparison between the simulated and measured S-parameters of the feeding network (a) when both diodes are OFF and (b) when D1 or D2 is ON.

values of the phase difference. Based on this plot, it is apparent that the proposed structure preserves its operating bandwidth despite the difference in phase between the received signals by the different elements. A similar response is obtained when inspecting the other curved or straight elements in both structures.

The total radiation efficiencies of C3 and S3 in both structures is found to be 0.81 and 0.87. The efficiency is computed at the resonant frequency of the corresponding element and by accounting for the coupling between C3 or S3 and all the remaining elements in both structures. Such efficiency is very similar to a standalone curved and dipole element. This proves that the diversity implementation does not deteriorate the radiation efficiency of each element due to the high isolation levels between the various dipoles.

## VII. Control of the System's Radiating Elements

The operation of each diversity structure is controlled by integrating a reconfigurable feeding network. The purpose of the network is to selectively enable each structure to radiate on demand, as illustrated in Fig. 14(a). The structure of the proposed reconfigurable feeding network is shown in Fig. 14(b). It is printed on a Rogers 3203 substrate with a dielectric constant of 3.02 and a thickness of 1.52 mm. It has an overall dimension of 3.5 cm × 3.5 cm and consists of three ports. Port 1 is the input port where the RF signal is supplied. The two output ports (Ports 2 and 3) are used to feed one straight and one curved dipole. Two p-i-n diodes ($D_1$ and $D_2$) are appropriately incorporated in the network's structure, as highlighted in Fig. 14(b). These p-i-n diodes allow the RF input signal to be delivered to either Port 2 or Port 3.

The reconfigurable feeding network is composed of multiple microstrip transmission lines with appropriate impedances to satisfy matching criteria. The first transmission line, where the input signal is supplied, has a width of 3.84 mm. This width corresponds to an input impedance of 50 Ω. The second transmission line has a length of 9.77 mm and a width of 1.8 mm. This length value is designed to match the 50 Ω input to the input impedance of the two p-i-n diodes ($D_1$ and $D_2$). The length of the second transmission corresponds to $\lambda_g/4$ at 5 GHz. The output of each p-i-n diode is connected to a 90° curved transmission line with a total length of 19.36 mm ($\lambda_g/2$ at 5 GHz) and a width of 2.34 mm. The last transmission line that is connected to Ports 2 and 3 has an impedance of 50 Ω. The activation of the two p-i-n diodes is done separately through an external bias tee that guides the RF signal and supplies the necessary dc current level. The p-i-n diodes used in this paper are BAR 64 from Infineon technologies [45]. Two biasing lines (lines 1 and 2), as highlighted in Fig. 14(b), are used to provide a closed path to the dc current that flows through each p-i-n diode from the external bias tee. Once connected to the ground of the feeding network, the corresponding p-i-n diode is activated. The fabricated prototype of the feeding network along with the biasing tee is shown in Fig. 14(c).

Fig. 15(a) compares the simulation and measurement of the reflection coefficient at the input port (Port 1), the reflection coefficient at the output port (Port 2), and the transmission from Port 1 to Port 2 when both diodes are OFF. There is no matching at the two ports. The corresponding reflection coefficients are higher than −10 dB. Besides reflection losses, a weak transmission is witnessed. This is due to the fact that during the OFF-mode, the diodes block the RF signal from being delivered to the corresponding output port. Fig. 15(b) shows the same data but for the case when diode $D_1$ is activated. The reflection coefficient at Port 1 and Port 2 is below −10 dB over the 4–6 GHz frequency span. The measured insertion loss is not more than −2 dB for the whole frequency range of interest.

Four networks are required to feed the different dipoles of both structures. The integration of the four networks with the antenna structure is demonstrated in Fig. 16(a). Each network is placed at the bottom layer of the antenna and orthogonal to the printed parasitic curved reflector. The ground plane of each feeding network is facing the corresponding

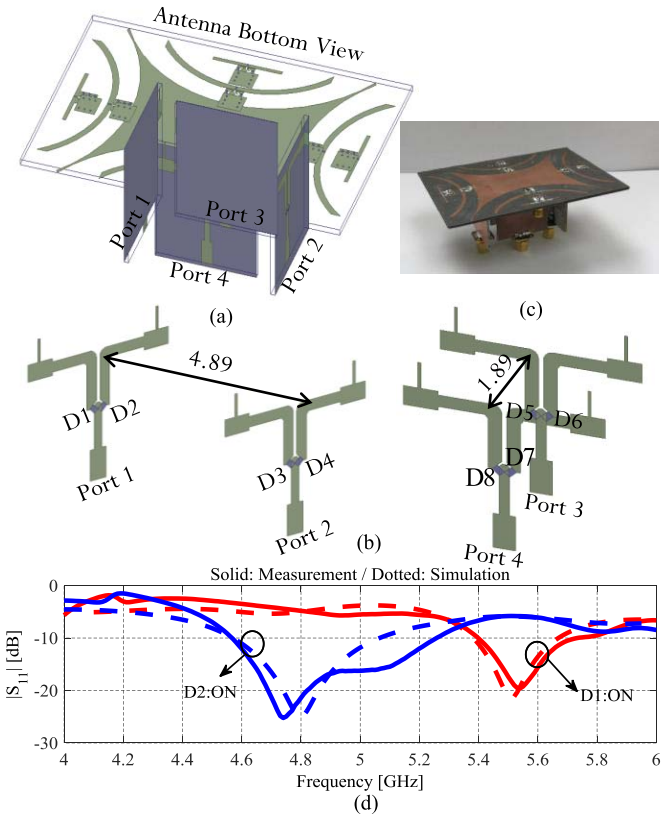


Fig. 16. (a) Bottom view of the integration of the four feeding networks underneath the curved printed reflector. (b) Location of the eight diodes within the four feeding networks. (c) Fabricated prototype. (d) Simulated and measured reflection coefficient.

set of dipole elements. Such placement guarantees that the radiation from the different antenna elements does not affect the operation of the four networks. Each feeding network contains two p-i-n diodes and in total four diodes must be activated simultaneously in order to feed either the four straight or curved elements. Diodes D1, D3, D5, and D7 that are shown in Fig. 16(b) must be activated simultaneously to feed all the four curved elements. The feeding of the four straight elements is done by biasing the other four diodes (D2, D4, D6, and D8). The corresponding fabricated prototype is shown in Fig. 16(c).

The comparison between the simulated and measured reflection coefficient at the input Port 1 of the feeding network is plotted in Fig. 16(d) when diode D1/D2 is forward biased. The simulation results are obtained by modeling the antenna system as an eight-port S-parameter matrix while each feeding network is modeled as a three-port S-parameter matrix. The connections between the two output ports of the feeding network and the antenna elements are achieved through low loss flexible coaxial cables. The lengths and losses of these cables are included in the simulation to account for their effect on the antenna matching performance. The same response can be obtained when activating the other diodes in the three different feeding networks. The measured isolations between the four inputs of the feeding networks when all the curved or straight elements are fed are summarized in Table III. The isolation is maintained below $-30$ dB between the different ports for both cases.

TABLE III

MEASURED ISOLATION $|S_{ij}|$ BETWEEN THE INPUT PORTS OF THE FOUR FEEDING NETWORKS

| Straight Dipoles ($f$=4.8 GHz) D2, D4, D6, D8: ON | Curved Dipoles ($f$=5.6 GHz) D1, D3, D5, D7: ON |
|---|---|
| $\|S_{12}\|_{dB}$=-36.4 | $\|S_{12}\|_{dB}$ =-38.2 |
| $\|S_{13}\|_{dB}$=-38.7 | $\|S_{13}\|_{dB}$ =-39.9 |
| $\|S_{34}\|_{dB}$=-32.5 | $S_{34}\|_{dB}$ =-35.2 |

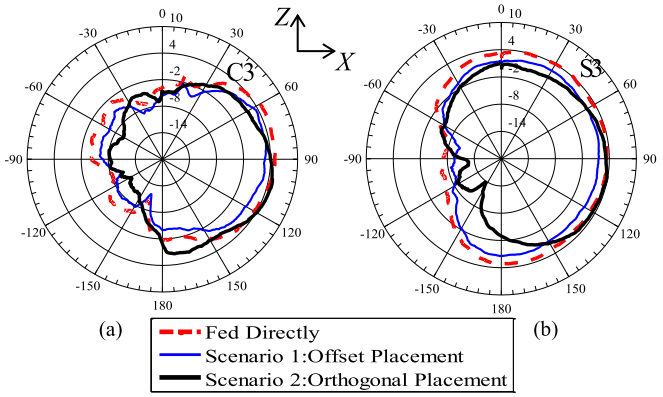


Fig. 17. Change in the measured gain pattern with and without the reconfigurable feeding network when feeding (a) C3 and (b) S3.

The total gain patterns for the various elements are affected by the integration of the four feeding networks within the antenna system. The transmission between the input port of each feeding network and one of its two output ports as well as the insertion loss of any biased p-i-n diode have an effect on the gain level of the corresponding radiating element. The measured gain pattern along the $xz$ plane when the curved element C3 is fed directly without the presence of the feeding network is shown in Fig. 17(a). The same data is plotted when C3 is fed through the third feeding network and by activating the diode D5. Two different scenarios for the feeding networks are investigated. The first scenario corresponds to the case when the feeding networks are not placed orthogonally to the printed curved reflector. The four feeding networks are located at an offset position away from the antenna structure. The purpose of this scenario is to assess the effect of the insertion loss of the reconfigurable feeding network on the antenna gain pattern. For this scenario, the measured total gain drops from 5.6 to 4.2 dBi. The second scenario, also shown in Fig. 17(a), assesses how the ground plane of each feeding network helps in compensating the drop in the gain levels. By placing the four reconfigurable feeding networks orthogonal to the printed parasitic reflector, the maximum achieved total gain for the curved elements increases to 5.3 dBi. The back lobe of the gain pattern also decreases. The same behavior is obtained for the remaining curved dipoles. Fig. 17(b) shows the same set of data but for the case when the straight element S3 is fed. The maximum measured total gain drops from 4.5 to 2.7 dBi after feeding the radiating element through the corresponding feeding network. The orthogonal placement of the four networks allows each straight dipole to achieve a maximum measured gain of 4.3 dBi with a decrease in the back lobe gain pattern. The direction of the maximum realized gain for

TABLE IV
COMPARISON BETWEEN THIS PAPER AND REFERENCES [6]–[12]

| | Nb. Of Diversity Antennas | Nb. Of Antenna Elements | Propag. Scenario | Polarization | Frequency Operation |
|---|---|---|---|---|---|
| [6] | 1 | 8 | Uniform | Single | Multiband |
| [7] | 1 | 4 | Uniform | Single | Multiband |
| [8] | 1 | 8 | Uniform | Dual | Single band |
| [9] | 1 | 4 | Uniform | Single | UWB |
| [10] | 1 | 4 | Uniform | Single | Single Band |
| [11] | 1 | 4 | Uniform | Dual | Multiband |
| [12] | 2 | 2/8 | Uniform | Single | Multiband |
| This work | 2 | 4/4 | Various Models | Dual | Frequency Reconfigurable |

both the curved and straight elements shifts from $\theta = 90°$ to almost $\theta = 110°$, as highlighted in Fig. 17. This shift is related to the placement of the feeding network orthogonally underneath the bottom layer of the antenna substrate.

As a summary, it is important to highlight the key differences between the work presented in this paper and recently published work on diversity antenna structures [6]–[12]. First, the system proposed in this paper features two compact antenna diversity structures that operate at two distinct spans of frequencies. Each antenna structure actively contributes in shaping the gain pattern of the other structure, thus improving the directional behavior of each antenna element and increasing the isolation levels between the different elements. This proposed paper is to our knowledge the first reported antenna system that features feeding reconfigurability between the two diversity structures. The reconfigurable feeding network is designed to choose which diversity structure to activate while at the same time compensate for all the losses that result from the activation of the integrated p-i-n diodes. A comparative analysis between this paper and previously published papers is summarized Table IV. Also in this paper, the diversity gains from each of the four curved or straight elements vary between 16.5 and 19.1 dB. As for [46], the authors are able to achieve a gain of 13.6 dB when relying on four folded dipole elements. The gain increases to 17 dB when adopting eight dual-polarized elements that operate at the same frequency. Another diversity antenna array that consists of eight antenna elements is discussed in [47]. The structure has four horizontally oriented and the remaining four are vertically oriented with a reported diversity gain of 9.5 dB.

## VIII. CONCLUSION

This paper presents an antenna system that is composed of different sets of curved and straight dipoles. The integration of a printed parasitic curved reflector is implemented to further improve the radiation characteristics of the various elements. The proposed system features good diversity for both structures in various propagation environments. A diversity gain between 16.5 and 19.1 dB is attained for a 1% probability level and by assuming a Rayleigh fading channel for both structures. Reconfigurable feeding networks are also incorporated within the antenna system to control which radiating structure is excited. The measurement results show good agreement with the simulated data, proving the validity of the proposed antenna system.

## REFERENCES


[1] S. Chen and K.-M. Luk, "A dual-mode wideband MIMO cube antenna with magneto-electric dipoles," *IEEE Trans. Antennas Propag.*, vol. 62, no. 12, pp. 5951–5959, Dec. 2014.

[2] W. Lin and H. Wong, "Polarization reconfigurable wheel-shaped antenna with conical-beam radiation pattern," *IEEE Trans. Antennas Propag.*, vol. 63, no. 2, pp. 491–499, Feb. 2015.

[3] C. Gu *et al.*, "Compact smart antenna with electronic beam-switching and reconfigurable polarizations," *IEEE Trans. Antennas Propag.*, vol. 63, no. 12, pp. 5325–5333, Dec. 2015.

[4] B. Wu and K.-M. Luk, "A 4-port diversity antenna with high isolation for mobile communications," *IEEE Trans. Antennas Propag.*, vol. 59, no. 5, pp. 1660–1667, May 2011.

[5] J. Oh and K. Sarabandi, "Compact, low profile, common aperture polarization, and pattern diversity antennas," *IEEE Trans. Antennas Propag.*, vol. 62, no. 2, pp. 569–576, Feb. 2014.

[6] Z. Qin, W. Geyi, M. Zhang, and J. Wang, "Printed eight-element MIMO system for compact and thin 5G mobile handest," *Electron. Lett.*, vol. 52, no. 6, pp. 416–418, 2016.

[7] M.-Y. Li *et al.*, "Eight-port orthogonally dual-polarized antenna array for 5G smartphone applications," *IEEE Trans. Antennas Propag.*, vol. 64, no. 9, pp. 3820–3830, Sep. 2016.

[8] Y.-L. Ban, C. Li, C.-Y.-D. Sim, G. Wu, and K.-L. Wong, "4G/5G multiple antennas for future multi-mode smartphone applications," *IEEE Access*, vol. 4, pp. 2981–2988, 2016.

[9] R. Anitha, P. V. Vinesh, K. C. Prakash, P. Mohanan, and K. Vasudevan, "A compact quad element slotted ground wideband antenna for MIMO applications," *IEEE Trans. Antennas Propag.*, vol. 64, no. 10, pp. 4550–4553, Oct. 2016.

[10] A. Ramachandran, S. V. Pushpakaran, M. Pezholil, and V. Kesavath, "A four-port MIMO antenna using concentric square-ring patches loaded with CSRR for high isolation," *IEEE Antennas Wireless Propag. Lett.*, vol. 15, pp. 1196–1199, 2016.

[11] D. Sarkar, A. Singh, K. Saurav, and K. V. Srivastava, "Four-element quad-band multiple-input–multiple-output antenna employing split-ring resonator and inter-digital capacitor," *IET Microw., Antennas Propag.*, vol. 9, no. 13, pp. 1453–1460, Oct. 2015.

[12] G. S. Reddy, A. Kamma, S. Kharche, J. Mukherjee, and S. K. Mishra, "Cross-configured directional UWB antennas for multidirectional pattern diversity characteristics," *IEEE Trans. Antennas Propag.*, vol. 63, no. 2, pp. 853–858, Feb. 2015.

[13] X. Zhang and L. Zhu, "Gain-enhanced patch antennas with loading of shorting pins," *IEEE Trans. Antennas Propag.*, vol. 64, no. 8, pp. 3310–3318, Aug. 2016.

[14] Y.-F. Lin, M.-J. Chang, H.-M. Chen, and B.-Y. Lai, "Gain enhancement of ground radiation antenna for RFID tag mounted on metallic plane," *IEEE Trans. Antennas Propag.*, vol. 64, no. 4, pp. 1193–1200, Apr. 2016.

[15] G. Zhai, Y. Cheng, Q. Yin, S. Zhu, and J. Gao, "Gain enhancement of printed log-periodic dipole array antenna using director cell," *IEEE Trans. Antennas Propag.*, vol. 62, no. 11, pp. 5915–5919, Nov. 2014.

[16] A. Dadgarpour, A. A. Kishk, and T. A. Denidni, "Gain enhancement of planar antenna enabled by array of split-ring resonators," *IEEE Trans. Antennas Propag.*, vol. 64, no. 8, pp. 3682–3687, Aug. 2016.

[17] L. Chen, Z. Lei, R. Yang, J. Fan, and X. Shi, "A broadband artificial material for gain enhancement of antipodal tapered slot antenna," *IEEE Trans. Antennas Propag.*, vol. 63, no. 1, pp. 395–400, Jan. 2015.

[18] H. Wang, S.-F. Liu, L. Chen, W.-T. Li, and X.-W. Shi, "Gain enhancement for broadband vertical planar printed antenna with H-shaped resonator structures," *IEEE Trans. Antennas Propag.*, vol. 62, no. 8, pp. 4411–4415, Aug. 2014.

[19] S. Soltani and R. D. Murch, "A compact planar printed MIMO antenna design," *IEEE Trans. Antennas Propag.*, vol. 63, no. 3, pp. 1140–1149, Mar. 2015.

[20] L. Zhao and K.-L. Wu, "A dual-band coupled resonator decoupling network for two coupled antennas," *IEEE Trans. Antennas Propag.*, vol. 63, no. 7, pp. 2843–2850, Jul. 2015.

[21] G. Zhai, Z. N. Chen, and X. Qing, "Enhanced isolation of a closely spaced four-element MIMO antenna system using metamaterial mushroom," *IEEE Trans. Antennas Propag.*, vol. 63, no. 8, pp. 3362–3370, Aug. 2015.

[22] M. Heino, S. N. Venkatasubramanian, C. Icheln, and K. Haneda, "Design of wavetraps for isolation improvement in compact in-band full-duplex relay antennas," *IEEE Trans. Antennas Propag.*, vol. 64, no. 3, pp. 1061–1070, Mar. 2016.

[23] M. N. Osman, M. K. Abdul Rahim, M. R. Hamid, M. F. M. Yusoff, and H. A. Majid, "Compact dual-port polarization-reconfigurable antenna with high isolations for MIMO application," *IEEE Antennas Wireless Propag. Lett.*, vol. 15, pp. 456–459, 2016.

[24] L. Zhao, L. K. Yeung, and K.-L. Wu, "A coupled resonator decoupling network for two-element compact antenna arrays in mobile terminals," *IEEE Trans. Antennas Propag.*, vol. 62, no. 5, pp. 2767–2776, May 2014.

[25] H. Lee and B. Lee, "Compact broadband dual-polarized antenna for indoor MIMO wireless communication systems," *IEEE Trans. Antennas Propag.*, vol. 64, no. 2, pp. 766–770, Feb. 2016.

[26] T. K. Roshna, U. Deepak, V. R. Sajitha, K. Vasudevan, and P. Mohanan, "A compact UWB MIMO antenna with reflector to enhance isolation," *IEEE Trans. Antennas Propag.*, vol. 63, no. 4, pp. 1873–1877, Apr. 2015.

[27] Y. Tawk, J. Costantine, and C. G. Christodoulou, "Cognitive-radio and antenna functionalities: A tutorial [wireless corner]," *IEEE Antennas Propag. Mag.*, vol. 56, no. 1, pp. 231–243, Feb. 2014.

[28] J.-S. Row and M.-J. Hou, "Design of polarization diversity patch antenna based on a compact reconfigurable feeding network," *IEEE Trans. Antennas Propag.*, vol. 62, no. 10, pp. 5349–5352, Oct. 2014.

[29] H. Sun and S. Sun, "A novel reconfigurable feeding network for quad-polarization-agile antenna design," *IEEE Trans. Antennas Propag.*, vol. 64, no. 1, pp. 311–316, Jan. 2016.

[30] J. F. Tsai and J. S. Row, "Reconfigurable square-ring microstrip antenna," *IEEE Trans. Antennas Propag.*, vol. 61, no. 5, pp. 2857–2860, May 2013.

[31] Y. F. Wu, C. H. Wu, D. Y. Lai, and F. C. Chen, "A reconfigurable quadri-polarization diversity aperture-coupled patch antenna," *IEEE Trans. Antennas Propag.*, vol. 55, no. 3, pp. 1009–1012, Mar. 2007.

[32] C. G. Christodoulou, Y. Tawk, S. A. Lane, and S. R. Erwin, "Reconfigurable antennas for wireless and space applications," *Proc. IEEE*, vol. 100, no. 7, pp. 2250–2261, Jul. 2012.

[33] Y. Tawk, J. Costantine, A. H. Ramadan, K. Y. Kabalan, and C. G. Christodoulou, "A reconfigurable feeding network," in *Proc. 8th Eur. Conf. Antennas Propag.*, The Hague, The Netherlands, Apr. 2014, pp. 1534–1536.

[34] Y. Tawk, C. G. Christodoulou, and J. Costantine, "An integrated two MIMO antenna system based on directive printed dipoles," in *Proc. IEEE Int. Symp. Antennas Propag. USNC/URSI Nat. Radio Sci. Meeting*, Vancouver, BC, Canada, Jul. 2015, pp. 705–706.

[35] *TDK Corporation (Part Number: HHM1732B1)*. Accessed: Jun. 2014. [Online]. Available: http://www.tdk.com

[36] C. A. Balanis, *Modern Antenna Handbook*. Hoboken, NJ, USA: Wiley, 2008.

[37] M. S. Sharawi, *Printed MIMO Antenna Engineering*. Norwood, MA, USA: Artech House, 2014.

[38] S. M. Moghaddam, A. A. Glazunov, P.-S. Kildal, J. Yang, and M. Gustafsson, "Improvement of an octave bandwidth bowtie antenna design based on the analysis of a MIMO efficiency metric in Random-Los," *Microw. Opt. Technol. Lett.*, vol. 59, no. 6, pp. 1229–1233, 2017.

[39] U. Carlberg, J. Carlsson, A. Hussain, and P.-S. Kildal, "Ray based multipath simulation tool for studying convergence and estimating ergodic capacity and diversity gain for antennas with given far-field functions," in *Proc. 20th Int. Conf. Appl. Electromagn. Commun.*, Dubrovnik, Croatia, Sep. 2010, pp. 1–4.

[40] P. S. Kildal, C. Orlenius, and J. Carlsson, "OTA testing in multipath of antennas and wireless devices with MIMO and OFDM," *Proc. IEEE*, vol. 100, no. 7, pp. 2145–2157, Jul. 2012.

[41] P.-S. Kildal and J. Carlsson, "New approach to OTA testing: RIMP and pure-LOS reference environments & a hypothesis," in *Proc. 7th Eur. Conf. Antennas Propag. (EuCAP)*, Gothenburg, Sweden, Apr. 2013, pp. 315–318.

[42] T. Taga, "Analysis for mean effective gain of mobile antennas in land mobile radio environments," *IEEE Trans. Veh. Technol.*, vol. 39, no. 2, pp. 117–131, May 1990.

[43] M. B. Knudsen and G. F. Pedersen, "Spherical outdoor to indoor power spectrum model at the mobile terminal," *IEEE J. Sel. Areas Commun.*, vol. 20, no. 6, pp. 1156–1169, Aug. 2002.

[44] A. Diallo, C. Luxey, P. L. Thuc, R. Staraj, and G. Kossiavas, "Diversity performance of multiantenna systems for UMTS cellular phones in different propagation environments," *Int. J. Antennas Propag.*, vol. 2008, Mar. 2008, Art. no. 836050.

[45] *Infineon Technologies (Part Number: BAR64-02V)*. Accessed: May 2014. [Online]. Available: http://www.infineon.com

[46] J. Yin, D. Nyberg, X. Chen, and P.-S. Kildal, "Characterization of multi-port eleven antenna for use in MIMO system," in *Proc. IEEE Int. Symp. Wireless Commun. Syst.*, Reykjavik, Iceland, Oct. 2008, pp. 473–477.

[47] S. K. Palaniswamy, Y. P. Selvam, M. G. N. Alsath, M. Kanagasabai, S. Kingsly, and S. Subbaraj, "3-D eight-port ultrawideband antenna array for diversity applications," *IEEE Antennas Wireless Propag. Lett.*, vol. 16, pp. 569–572, 2017.

**Youssef Tawk** received the bachelor's degree in computer and communication engineering (highest distinction) from Notre Dame University, Louaize, Zouk Mosbeh, Lebanon, in 2006, the master's degree in electrical and computer engineering from the American University of Beirut, Beirut, Lebanon, in 2008, and the Ph.D. degree from the University of New Mexico, Albuquerque, NM, USA, in 2011.

He was a Post-Doctoral Researcher and then Research Professor with the University of New Mexico. He is an Assistant Professor with the Electrical and Computer Engineering Department, Notre Dame University, Louaize. He has authored or co-authored several journal and conference papers many of which received finalist positions and honorable mentions in several paper contests. He has co-authored two books and one book chapter as well as several patents. His current research interests include cognitive radio, reconfigurable RF systems, deployable antennas, microwave engineering, and millimeter-wave technology.

Dr. Tawk was a recipient of many awards and honors throughout his career and studies.

**Joseph Costantine** received the bachelor's degree in electrical, electronics, computer and communications engineering from the second branch of the Faculty of Engineering, Lebanese University, Beirut, Lebanon, in 2004, the master's degree in computer and communications engineering from the American University of Beirut, Beirut, Lebanon, in 2006, and the Ph.D. degree from the University of New Mexico, Albuquerque, NM, USA, in 2009.

He was a Post-Doctoral Researcher with the University of New Mexico. He was an Assistant Professor with California State University, Fullerton, CA, USA. He is an Associate Professor with the Electrical and Computer Engineering, American University of Beirut. He has authored or co-authored many research papers, two books, and one book chapter. He holds several patents. His current research interests include reconfigurable antennas for Internet of Things and compact devices, cognitive radio, RF systems for biomedical applications, RF energy harvesting, and deployable antennas for small satellites.

Dr. Costantine was a recipient of many awards including the summer faculty fellowship from the Space Vehicles Directorate, Albuquerque, NM, USA, for three consecutive years.

**Christos G. Christodoulou** (F'02) received the Ph.D. degree in electrical engineering from North Carolina State University, Raleigh, NC, USA, in 1985.

He was a Faculty Member with the University of Central Florida, Orlando, FL, USA, from 1985 to 1998. In 1999, he joined the faculty of the Electrical and Computer Engineering Department, the University of New Mexico (UNM), Albuquerque, NM, USA, where he was the Chair of the Department from 1999 to 2005. He is currently the Dean of the School of Engineering and Computing at the UNM. He has authored or co-authored over 500 papers in journals and conferences, 17 book chapters, and 8 books. He holds several patents. His current research interests include modeling of electromagnetic systems, machine learning in electromagnetics, high-power microwave antennas, reconfigurable antennas for cognitive radio, and RF/Photonics.

Dr. Christodoulou is a member of Commission B of the U.S. National Committee for URSI and a Distinguished Professor at UNM. He was a recipient of the 2010 IEEE John Krauss Antenna Award for his work on reconfigurable fractal antennas using MEMS switches, the Lawton-Ellis Award, the Gardner Zemke Professorship at the University of New Mexico, and the IEEE Outstanding Engineering Educator in 2012 (Albuquerque Section). He has been inducted in the Alumni Hall of Fame for the Electrical and Computer Engineering Department, North Carolina State University, in 2016. He was an IEEE AP-S Distinguished Lecturer from 2007 to 2010. He was an Associate Editor of the IEEE TRANSACTIONS ON ANTENNAS AND PROPAGATION for six years. He served as a Co-Editor for a special issue on "Reconfigurable Systems" in the IEEE PROCEEDINGS in 2015, for a special issue on "Synthesis and Optimization Techniques in Electromagnetics and Antenna System Design" in the IEEE ANTENNAS AND PROPAGATION in 2007, and for the special issue on "Antenna Systems and Propagation for Cognitive Radio" in 2014. Since 2013, he has been serving as the Series Editor for Artech House Publishing Company in the area of antennas and propagation.